Geochemical Perspectives Letters

K, Rb, Ge, and Cu isotopes in Oued Chebeika 002 compared with CI chondrites, Ryugu, and Bennu

D.S. Grewal[1*], N.X. Nie[2*], B. Luais[3*], Z.J. Zhang[2*], Q. Ahmad[3], A. Vazquez Ochoa[4], P. Ni[4*]

OPEN ACCESS

https://doi.org/10.7185/geochemlet.2618

Abstract

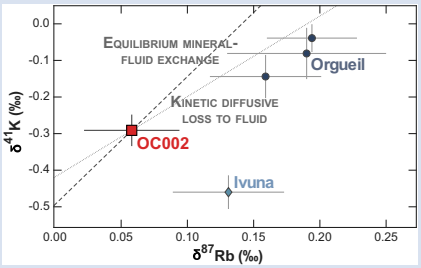

The primordial isotopic compositions of moderately volatile elements in CI chondrites may be obscured by aqueous alteration on their parent bodies. Here we report K, Rb, Ge, and Cu isotopic compositions of Oued Chebeika 002 (OC002), a CI chondrite recovered shortly after its fall and thus minimally affected by terrestrial weathering. OC002 exhibits light $\delta^{41/39}$K (−0.291 ± 0.043 ‰), comparable to Bennu and lighter than other CI chondrites and Ryugu, and the lightest $\delta^{87/85}$Rb (+0.058 ± 0.036 ‰) yet measured in a CI chondrite. Meanwhile, its $\delta^{74/70}$Ge (+0.980 ± 0.042 ‰) and $\delta^{65/63}$Cu (+0.197 ± 0.020 ‰) values fall within the CI-Ryugu field. This element specific pattern – K and Rb variable, Ge and Cu uniform – indicates that parent body aqueous alteration selectively fractionated fluid mobile alkalis whereas Ge and Cu isotopes remained largely insensitive. The range of K and Rb isotopic composition in CI chondrites spans nearly the total variation observed across carbonaceous chondrite groups, implying that $\delta^{41/39}$K and $\delta^{87/85}$Rb of the CI end member cannot be uniquely defined. This introduces significant uncertainty when using CI chondrites as the matrix end member to constrain chondrule isotopic compositions for fluid mobile elements. More broadly, our results demonstrate that "pristine" with respect to terrestrial weathering does not equal "primitive" with respect to parent body processing.

Received 8 February 2026 | Accepted 27 April 2026 | Published 11 June 2026

Introduction

Ivuna-type (CI) chondrites are the most chemically primitive meteorites, with elemental abundances matching solar photosphere values for all but the most volatile elements (Lodders, 2003). However, this chemical primitiveness belies a complex alteration history: CI chondrites are derived from ice-rich planetesimals which underwent pervasive aqueous alteration, which can produce isotopic heterogeneity within the parent body (Hu *et al.*, 2024; Barnes *et al.*, 2025) and likely renders efforts to define the primordial isotopic composition of the CI group prone to sampling bias. This heterogeneity is particularly consequential for the mass dependent isotopic compositions of moderately volatile elements (MVEs; 50 % condensation temperatures between ~1300 and 650 K). Chondrule-free CI chondrites represent the isotopically "heavy" end member relative to other carbonaceous chondrites, which are mixtures of a CI-like matrix and isotopically light chondrules (Nie *et al.*, 2021; Zhang and Grewal, 2026). Since CI values are used as the matrix end member to constrain the MVE isotopic composition of the chondrule component, any internal variability in CI chondrites directly propagates into uncertainty in the calculated chondrule composition. Yet the extent of this variability, and whether it reflects parent body aqueous alteration, terrestrial weathering, or both, remains poorly constrained.

Among MVEs, K, Rb, Ge, and Cu isotopes have been critical for constraining chondrule formation conditions (Nie *et al.*, 2021; Zhang and Grewal, 2026), yet they record distinct aspects of parent body processing due to their differing geochemical affinities. Lithophile K and Rb are highly fluid mobile and thus sensitive to aqueous alteration (Pringle and Moynier, 2017; Koefoed *et al.*, 2023; Nie *et al.*, 2023; Hu *et al.*, 2024; Barnes *et al.*, 2025), whereas siderophile Ge and chalcophile Cu are hosted in phases less susceptible to fluid mobilisation (Luck *et al.*, 2005; Barnes *et al.*, 2025; Luais and Florin, 2025; Wölfer *et al.*, 2025a). Such contrasting behaviours mean these isotopic systems respond differently to aqueous alteration; however, distinguishing parent body effects from terrestrial weathering in historical falls like Orgueil (1864) and Ivuna (1938), which may have experienced alteration during prolonged storage, remains challenging. For instance, $\delta^{41/39}$K values in Orgueil span from −0.581 to −0.039 ‰ (Wang and Jacobsen, 2016; Ku and Jacobsen, 2020; Nie *et al.*, 2021; Koefoed *et al.*, 2023) (Fig. 1a), and Ivuna shows a similarly broad range of −0.460 to −0.180 ‰ (Nie *et al.*, 2021; Koefoed *et al.*, 2023) (Fig. 1a). In contrast, Ryugu samples define a narrower and heavier range (−0.207 ‰ to −0.172 ‰; Hu *et al.*, 2024), while Bennu yields a lighter value of −0.380 ± 0.026 ‰ (Barnes *et al.*, 2025). The situation is even more poorly constrained for Rb isotopes, where data exist only for Orgueil and Ivuna (Pringle and Moynier, 2017; Nie *et al.*, 2021) (Fig. 1b), with no measurements for

1. Department of Earth and Planetary Sciences, Yale University, New Haven, CT 06511, USA
2. CAT Lab, Department of Earth, Atmospheric, and Planetary Sciences, Massachusetts Institute of Technology, Cambridge, MA 02139, USA
3. Université de Lorraine, CNRS, CRPG, Nancy, F-54000, France
4. Department of Earth, Planetary, and Space Sciences, University of California, Los Angeles, Los Angeles, CA 90095, USA
* Corresponding authors (email: damanveer.grewal@yale.edu; nxnie@mit.edu, beatrice.luais@univ-lorraine.fr, zhez@mit.edu, pengni@epss.ucla.edu)

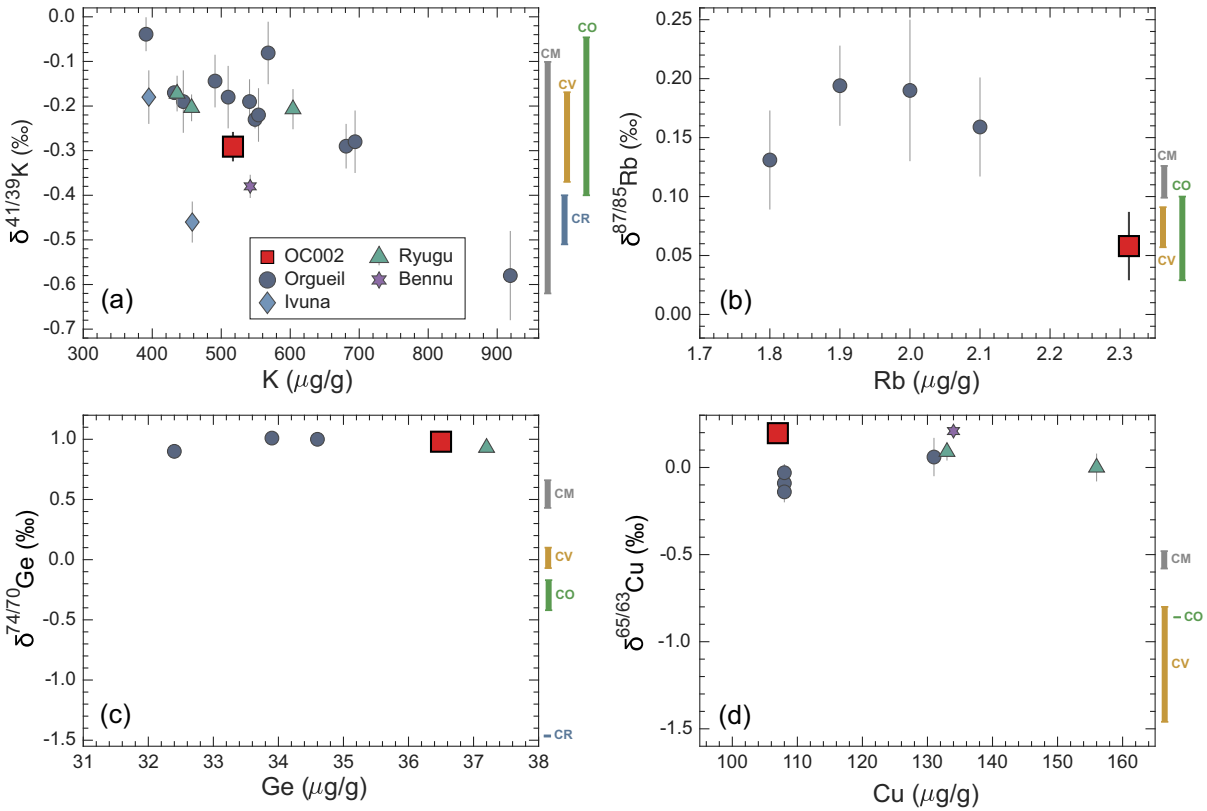

Figure 1 Isotopic compositions *versus* concentrations for **(a)** K, **(b)** Rb, **(c)** Ge, and **(d)** Cu in OC002, other CI chondrites, Ryugu, and Bennu. OC002 exhibits light $\delta^{41/39}$K and $\delta^{87/85}$Rb relative to other CI chondrites and Ryugu, while the $\delta^{74/70}$Ge and $\delta^{65/63}$Cu fall within the CI-Ryugu field. On the right side of each plot, the ranges of isotopic compositions for other carbonaceous chondrite groups are shown for comparison. OC002 data from this study; literature data from Wang and Jacobsen (2016), Pringle and Moynier (2017), Ku and Jacobsen (2020), Nie *et al.* (2021), Koefoed *et al.* (2023), Paquet *et al.* (2023), Hu *et al.* (2024), Barnes *et al.* (2025), Luais and Florin (2025), Wölfer *et al.* (2025a,b). Error bars represent 2 s.d. or 95 % c.i.; where not visible, they are smaller than the symbol size.

Ryugu or Bennu. Whether this variability among CI-like materials reflects aqueous alteration on their parent bodies or, in the case of historical meteorite falls, remobilisation during terrestrial residence remains unclear. Constraining the MVE isotopic compositions of additional pristine CI samples is therefore critical.

The discovery of Oued Chebeika 002 (OC002) in Morocco in 2024 provides an excellent opportunity to address these uncertainties. Recovered shortly after falling in a hot desert, OC002 has experienced negligible terrestrial weathering, making it comparable to samples returned from asteroids Ryugu and Bennu (Gattacceca *et al.*, 2025; Zhu *et al.*, 2025). Here, we report K, Rb, Ge, and Cu isotopic compositions of OC002 and compare them with other CI chondrites to evaluate (1) the extent of isotopic heterogeneity among CI chondrites, and (2) its implications for constraining the chondrule component using CI end member compositions.

Samples and Methods

A ~260 mg aliquot of OC002 was purchased from the same batch of mm sized fragments analysed by Gattacceca *et al.* (2025). Given the broadly homogeneous bulk elemental composition of CI chondrites at the mg scale, separate aliquots were used for Ge and K + Rb + Cu isotope systems at different laboratories. ~200 mg was allocated for Ge isotope and chemical composition analyses at Université de Lorraine. The remaining material was homogenised, after which ~50 mg was used for K and Rb isotope analyses at MIT, and ~4 mg was used for Cu isotope analyses at UCLA. Sample digestion, chemical separation, and isotope measurements followed established procedures [(K, Rb: Nie *et al.*, 2021; Zhang *et al.*, 2025); (Ge: Luais, 2012; Luais and Florin, 2025; Ahmad *et al.*, 2026); (Cu: Ni *et al.*, 2021)], with details provided in Supplementary Information. Isotopic compositions are reported in delta notation (‰) relative to certified standards (SRM 999c for K, SRM 984 for Rb, NIST SRM 3120a for Ge, and SRM 976 for Cu). Uncertainties are 95 % confidence intervals (c.i.) based on repeated measurements (n = 5–7) of each sample solution, assuming a Student's t distribution. Major and trace element compositions are reported in Table S-1.

Results

The K, Rb, Ge, and Cu concentrations and isotopic compositions of OC002 are reported in Table 1. OC002 yields $\delta^{41/39}$K of −0.291 ± 0.043 ‰, lower than the Ryugu mean (−0.194 ± 0.038 ‰; Hu *et al.*, 2024), and the heavier Orgueil values (−0.183 to −0.039 ‰; Ku and Jacobsen, 2020; Nie *et al.*, 2021; Koefoed *et al.*, 2023; Hu *et al.*, 2024), but comparable to the lighter Orgueil measurements (−0.29 to −0.28 ‰; Koefoed *et al.*, 2023) and Bennu (−0.380 ± 0.026 ‰; Barnes *et al.*, 2025) (Fig. 1a). OC002 is heavier than both the lightest Ivuna (−0.460 ± 0.046 ‰; Nie *et al.*, 2021) and Orgueil (−0.581 ± 0.097 ‰; Wang and Jacobsen, 2016) values. The $\delta^{87/85}$Rb of OC002 is +0.058 ± 0.036 ‰, lower than Ivuna (+0.131 ± 0.042 ‰; Nie *et al.*, 2021) and Orgueil (+0.159 to +0.194 ‰; Nie *et al.*, 2021; Pringle and Moynier, 2017), representing the lightest Rb isotopic composition yet measured in a CI chondrite (Fig. 1b). In contrast, the Cu and Ge isotopic compositions of OC002 closely match

Table 1 Isotopic compositions and concentrations of K, Rb, Ge, and Cu.

	δ (‰)	Count	2 s.d.	c.i. (95 %)	Concentration (μg/g)
$^{41/39}$K	−0.291	6	0.082	0.043	525
$^{87/85}$Rb	0.058	7	0.078	0.036	2.3
$^{74/70}$Ge	0.980	5	0.067	0.042	36.5
$^{65/63}$Cu	0.197	6	0.038	0.020	107

those of other CI chondrites and Ryugu (Fig. 1c,d). The $\delta^{74/70}$Ge value (+0.980 ± 0.042 ‰) falls within the CI-Ryugu range (+0.901 to +1.010 ‰; Luais and Florin, 2025; Wölfer *et al.*, 2025a,b). The $\delta^{65/63}$Cu (+0.197 ± 0.020 ‰) is comparable to Bennu (+0.209 ± 0.015 ‰; Barnes *et al.*, 2025) and Alais (+0.17 ± 0.03 ‰; Paquet *et al.*, 2023), lying at the upper end of the CI-Ryugu range (−0.09 to +0.17 ‰; Luck *et al.*, 2005; Paquet *et al.*, 2023).

Discussion

OC002 reveals an element specific pattern in MVE isotopes: K and Rb are isotopically lighter relative to CI-Ryugu averages, whereas Ge and Cu remain within the CI-Ryugu field.

Because CI-like materials are essentially chondrule-free, this variability cannot be attributed to differing proportions of primordial nebular components. Instead, given that these materials are heavily aqueously altered, the coupled light isotopic signatures in both K and Rb most likely reflect selective redistribution of fluid mobile alkalis during aqueous processing on their parent bodies.

Coupled K-Rb isotopic systematics: parent body or terrestrial aqueous alteration? Among the five CI samples with paired K and Rb isotope data (Pringle and Moynier, 2017; Nie *et al.*, 2021; Hu *et al.*, 2024), OC002 exhibits light $\delta^{41/39}$K and $\delta^{87/85}$Rb values, while three Orgueil samples cluster at heavier values (Fig. 2). These four samples define a positive $\delta^{41/39}$K-$\delta^{87/85}$Rb correlation, consistent with a common fractionation process affecting both alkali elements. Terrestrial weathering studies suggest that aqueous fluids preferentially incorporate heavier K isotopes relative to coexisting silicates, with apparent fractionation of up to ~0.6 ‰ documented in weathering profiles (Chen *et al.*, 2020) and theoretical calculations predicting ~0.24 ‰ fractionation between aqueous K^+ and clay minerals at 298 K (Zeng *et al.*, 2019). Because K and Rb share similar ionic radii, coordination chemistry, and residence in phyllosilicate interlayer sites, Rb is expected to follow K during fluid-rock interaction (Zeng *et al.*, 2019). The predicted equilibrium $\delta^{41/39}$K/$\delta^{87/85}$Rb slope is ~3.5, while kinetic diffusion in water yields a slope of ~2.2 (Zeng *et al.*, 2019). Excluding Ivuna, OC002 and the three Orgueil samples define a slope consistent with kinetic fractionation (Fig. 2), suggesting that diffusion controlled processes, such as ion migration within phyllosilicates or at mineral-fluid interfaces, dominated alkali redistribution during aqueous alteration.

Although the fractionation direction would be identical for both parent body and terrestrial aqueous alteration, several observations favour a parent body origin for OC002's light K and Rb isotopic signatures. OC002 was recovered shortly after its fall and exhibits minimal terrestrial weathering, with preserved fusion crust, absence of sulfates and ferrihydrite, and mineralogy indistinguishable from Ryugu and Bennu (Gattacceca *et al.*, 2025). Bennu samples, entirely free from terrestrial weathering, yield comparably light $\delta^{41/39}$K (Barnes *et al.*, 2025), reinforcing that such signatures are intrinsic to CI-like materials. The K and Rb abundances of OC002 fall within the normal CI range (Fig. 1a,b), consistent with parent body isotopic redistribution rather than terrestrial addition or leaching. Furthermore, the $\delta^{87/85}$Rb of OC002 distinguishes it from common terrestrial materials, which have much lower $\delta^{87/85}$Rb values (−0.23 to −0.11 ‰; Nie *et al.*, 2021; Zhang *et al.*, 2025). The Ivuna sample analysed by Nie *et al.* (2021) plots off the OC002-Orgueil trend, exhibiting one of the lightest $\delta^{41/39}$K among all CI chondrites yet only intermediate $\delta^{87/85}$Rb (Fig. 2). This decoupling likely reflects either that its K and Rb isotopes were fractionated at different times or by different processes, or sampling of lithologically distinct material within the brecciated CI regolith.

Constraints from Ge and Cu isotopes. The contrasting behaviour of Ge and Cu compared to K and Rb provides independent constraints on the origin of alkali isotope heterogeneity. The $\delta^{74/70}$Ge and $\delta^{65/63}$Cu values of OC002 fall within the CI-Ryugu-Bennu field despite its light K and Rb isotopic signatures. Although Ge is siderophile, CI chondrites lack metal phases due to pervasive aqueous alteration; instead, Ge substitutes for Si in the tetrahedral sites of phyllosilicates and silicates (Rouxel and Luais, 2017), where it is structurally bound rather than exchangeable and thus essentially immobile during low temperature fluid-rock interaction. Copper, primarily hosted in sulfides, remains isotopically homogeneous at the bulk sample scale in CI chondrites, Ryugu, and Bennu (Paquet *et al.*, 2023; Barnes *et al.*, 2025), likely reflecting efficient local re-equilibration. The total isotopic variations in Ge and Cu across carbonaceous chondrites are much larger than those of K and Rb (Fig. 1), possibly

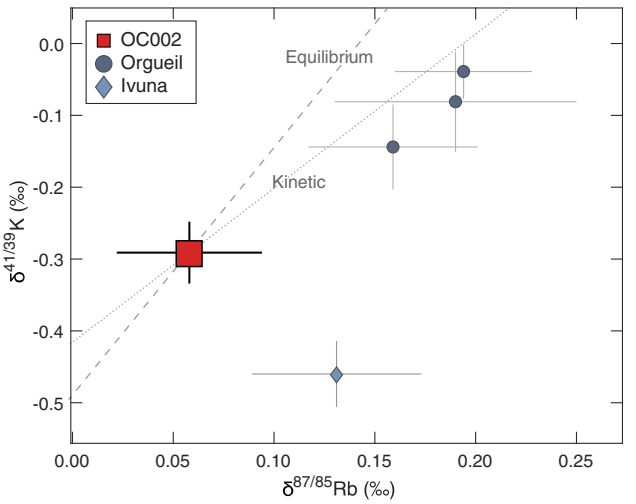

Figure 2 Coupled $\delta^{41/39}$K and $\delta^{87/85}$Rb for CI chondrites with paired measurements from the same aliquots. OC002 (this study), Orgueil and Ivuna data from Pringle and Moynier (2017), Nie *et al.* (2021), and Hu *et al.* (2024). OC002 and Orgueil define a positive correlation consistent with fluid mediated alkali fractionation; Ivuna plots off this trend. Dashed and dotted lines represent slopes predicted $\delta^{41/39}$K/$\delta^{87/85}$Rb slopes for equilibrium fractionation (3.5) and kinetic fractionation due to diffusion in water (2.2), respectively (Zeng *et al.*, 2019). Error bars represent 2 s.d. or 95 % c.i.

reflecting their higher volatility and thus more fractionated chondrule isotopic compositions (Zhang and Grewal, 2026). Any isotopic effects of aqueous alteration on Ge and Cu are therefore small relative to intergroup variations.

This element specific pattern – alkali isotopes variable, and Ge and Cu isotopes uniform – indicates that K and Rb isotopic heterogeneity in CI chondrites reflects selective mobilisation of elements hosted in exchangeable phyllosilicate interlayer sites rather than heterogeneous nebular inheritance. The latter would produce correlated variations across all isotope systems, which is not observed. Instead, K and Rb isotopes record parent body aqueous redistribution, while Ge and Cu were not significantly affected. This interpretation is independently supported by Barnes *et al.* (2025), who observed similar decoupling – variable K but uniform Cu – in Bennu samples.

The challenge of constraining primordial K and Rb isotopic compositions. Although aqueous alteration is clearly implicated in K and Rb isotope variability in CI chondrites, knowing the direction of fractionation does not resolve a more fundamental problem: what was the primordial K and Rb isotopic composition of the CI group before alteration occurred? A sample with relatively heavy K isotopic composition could represent either material that retained heavy isotope-enriched fluids or material that experienced minimal fluid-rock interaction and better preserves the primordial signature. Conversely, a sample with light K isotopic composition could represent residual material from which heavy isotope-enriched fluids were extracted, with the isotopic shift reflecting the extent of fluid loss. Without independent constraints on fluid fluxes, which K and Rb abundances and isotopes alone cannot provide, the pre-alteration $\delta^{41/39}$K and $\delta^{87/85}$Rb values in CI chondrites remain indeterminate. Isotopic shifts of the magnitude observed (~0.5 ‰ and ~0.15 ‰ range in $\delta^{41/39}$K and $\delta^{87/85}$Rb, respectively) could bias any calculated average either light or heavy relative to the true primordial composition, depending on whether sampled CI materials were net fluid loss or fluid gain systems.

Implications for chondrule-matrix mixing models. The recognition that CI chondrites exhibit resolvable K and Rb isotopic variability has important implications for chondrule-matrix mixing models. These models constrain chondrule and matrix end member isotopic compositions by regressing bulk chondrite isotopic compositions against matrix mass fractions, with end member values determined by the intercepts (Luais and Florin, 2025; Nie *et al.*, 2021; Wölfer *et al.*, 2025a; Zhang and Grewal, 2026). CI chondrites, being 100 % matrix, plot at the high matrix fraction end of such regressions. Our data indicate that caution is warranted when including CI chondrites in K and Rb regressions. The range of $\delta^{41/39}$K values in CI chondrites (−0.58 to −0.04 ‰) spans nearly the total variation observed across other carbonaceous chondrite groups (−0.62 to −0.10 ‰; Bloom *et al.*, 2020; Nie *et al.*, 2021; Koefoed *et al.*, 2023; Hu *et al.*, 2024) (Fig. 3a). Similar variability is observed for Rb (Fig. 3b). This scatter at the matrix-rich end propagates into the uncertainty of both end member intercepts. Although the slopes of mixing arrays may still encode chondrule-matrix proportions, the inferred intercepts are only as robust as the data constraining them.

One approach to mitigate this limitation might be to exclude CI chondrites and use only other carbonaceous chondrite groups for regressions. However, the problem extends beyond CI chondrites. Previous studies have documented large intra-group $\delta^{41/39}$K variability in several carbonaceous chondrite groups, with scatter that can occur without corresponding variability in less mobile isotopic systems (Nie *et al.*, 2021; Hu *et al.*, 2024; Barnes *et al.*, 2025) (Fig. 3a). Similar behaviour is observed for fluid mobile highly volatile elements such as C and N, whose isotopic compositions show substantial intra-group variability in carbonaceous chondrites (Grewal, 2022; Grewal *et al.*, 2022, 2025; Grewal and Mukhopadhyay, 2025). This pattern is also evident in that K abundances display pronounced scatter among CM chondrites (Braukmüller *et al.*, 2018), irrespective of fall/find classification, indicating that alkali abundances can vary significantly even within a single group. These observations suggest that for K and Rb, aqueous alteration introduces sample scale heterogeneity that makes the bulk isotopic composition of any carbonaceous chondrite group difficult to constrain precisely – unlike isotopic systems less sensitive to fluid redistribution, such as Ge and Cu.

Previous studies have attempted to address CI variability by defining a best estimate CI $\delta^{41/39}$K from Orgueil, Ivuna, and Ryugu, treating the anomalously light Ivuna value as an outlier (Koefoed *et al.*, 2023; Hu *et al.*, 2024). However, this approach implicitly assumes that averaging captures the pre-alteration value – an assumption that cannot be validated without independent constraints on fluid flux history. If fluid extraction was systematically unidirectional across the CI reservoir

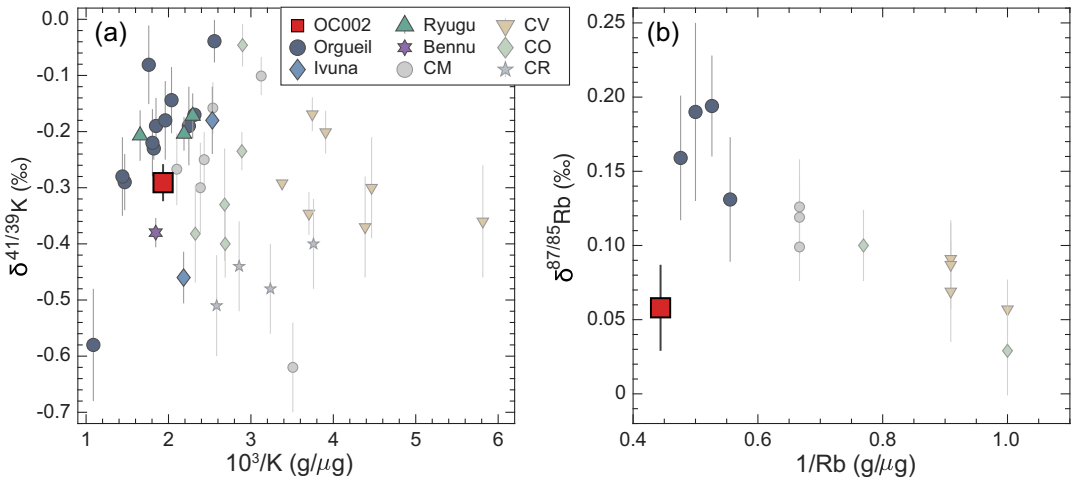

Figure 3 Isotopic compositions *versus* inverse concentrations for **(a)** K and **(b)** Rb in carbonaceous chondrites. The range of $\delta^{41/39}$K and $\delta^{87/85}$Rb in CI chondrites (including OC002) spans nearly the total variation observed across other carbonaceous chondrite groups. Data sources are in Figure 1.

(Hu *et al.*, 2024), even a carefully constructed average could be biased. The practical outcome is that CI chondrites should be treated not as a single point but as a bounded field for fluid mobile elements such as K and Rb.

Our results underscore a broader conclusion: "pristine" with respect to terrestrial weathering does not equal "primitive" with respect to parent body alteration. OC002, despite being among the least terrestrially altered CI chondrites yet recovered, records a K and Rb isotopic signature that deviates from the proposed CI group average – evidence that aqueous alteration on CI parent bodies has introduced irreducible heterogeneity into the alkali isotope record.

Acknowledgements

The authors thank Rayssa Martins and Kun Wang for their constructive comments. BL and QA thank D. Cividini for technical assistance with the Ge isotopes analyses at CRPG. This study was supported by start-up funds provided by Yale University to DSG; NASA grants (80NSSC23K1163 and 80NSSC24K1785), a Research Innovation Seed Fund and start-up funds provided by MIT to NXN; ANR-FRANCE (French National Research Agency) project *Planet*GEM (Grant# ANR-21-CE49-0011) to BL; and a NASA grant (80NSSC25K7918) to PN.

Editor: Helen Williams

Author Contributions

Conceptualisation: DSG, NXN, BL, PN. **Methodology**: NXN, BL, ZJZ, QA, PN. **Investigation**: ZJZ, BL, PN, NXN, AVO. **Writing-original draft**: DSG. **Writing-review and editing**: DSG, NXN, BL, PN.

Additional Information

Supplementary Information accompanies this letter at https://www.geochemicalperspectivesletters.org/article2618.

Cite this letter as: Grewal, D.S., Nie, N.X., Luais, B., Zhang, Z.J., Ahmad, Q., Vazquez Ochoa, A., Ni, P. (2026) K, Rb, Ge, and Cu isotopes in Oued Chebeika 002 compared with CI chondrites, Ryugu, and Bennu. *Geochem. Persp. Let.* 40, 24–29. https://doi.org/10.7185/geochemlet.2618

References

Ahmad, Q., Cividini, D., Luais, B. (2026) A fast double-stack chromatographic separation of germanium from silicate material for isotope analysis with MC-ICP-MS. *Journal of Analytical Atomic Spectrometry* 41, 935–941. https://doi.org/10.1039/D5JA00471C

Barnes, J.J., Nguyen, A.N., Abernethy, F.A.J., Bajo, K., Bekaert, D.V., *et al.* (2025) The variety and origin of materials accreted by Bennu's parent asteroid. *Nature Astronomy* 9, 1785–1802. https://doi.org/10.1038/s41550-025-02631-6

Bloom, H., Lodders, K., Chen, H., Zhao, C., Tian, Z., Koefoed, P., Petö, M.K., Jiang, Y., Wang, K.(王昆) (2020) Potassium isotope compositions of carbonaceous and ordinary chondrites: Implications on the origin of volatile depletion in the early solar system. *Geochimica et Cosmochimica Acta* 277, 111–131. https://doi.org/10.1016/j.gca.2020.03.018

Braukmüller, N., Wombacher, F., Hezel, D.C., Escoube, R., Münker, C. (2018) The chemical composition of carbonaceous chondrites: Implications for volatile element depletion, complementarity and alteration. *Geochimica et Cosmochimica Acta* 239, 17–48. https://doi.org/10.1016/j.gca.2018.07.023

Chen, H., Liu, X.-M., Wang, K. (2020) Potassium isotope fractionation during chemical weathering of basalts. *Earth and Planetary Science Letters* 539, 116192. https://doi.org/10.1016/j.epsl.2020.116192

Gattacceca, J., Gounelle, M., Devouard, B., Barrat, J.-A., Bonal, L., *et al.* (2025) Oued Chebeika 002: A new CI1 meteorite linked to outer solar system bodies. *Meteoritics & Planetary Science* 60, 1441–1479. https://doi.org/10.1111/maps.14359

Grewal, D.S. (2022) Origin of Nitrogen Isotopic Variations in the Rocky Bodies of the Solar System. *The Astrophysical Journal* 937, 123. https://doi.org/10.3847/1538-4357/ac8eb4

Grewal, D.S., Mukhopadhyay, S. (2025) Using carbon isotopes to trace the origin of volatiles on Earth and Mars. *Geochimica et Cosmochimica Acta* 408, 12–27. https://doi.org/10.1016/j.gca.2025.09.014

Grewal, D.S., Seales, J.D., Dasgupta, R. (2022) Internal or external magma oceans in the earliest protoplanets – Perspectives from nitrogen and carbon fractionation. *Earth and Planetary Science Letters* 598, 117847. https://doi.org/10.1016/j.epsl.2022.117847

Grewal, D.S., Bhattacharjee, S., Mardaru, G.-D., Asimow, P.D. (2025) Tracing the origin of volatiles on Earth using nitrogen isotope ratios in iron meteorites. *Geochimica et Cosmochimica Acta* 388, 34–47. https://doi.org/10.1016/j.gca.2024.11.011

Hu, Y., Moynier, F., Dai, W., Paquet, M., Yokoyama, T., *et al.* (2024) Pervasive aqueous alteration in the early Solar System revealed by potassium isotopic variations in Ryugu samples and carbonaceous chondrites. *Icarus* 409, 115884. https://doi.org/10.1016/j.icarus.2023.115884

Koefoed, P., Barrat, J.-A., Pravdivtseva, O., Alexander, C.M.O'D., Lodders, K., Ogliore, R., Wang, K. (王昆) (2023) The potassium isotopic composition of CI chondrites and the origin of isotopic variations among primitive planetary bodies. *Geochimica et Cosmochimica Acta* 358, 49–60. https://doi.org/10.1016/j.gca.2023.07.025

Ku, Y., Jacobsen, S.B. (2020) Potassium isotope anomalies in meteorites inherited from the protosolar molecular cloud. *Science Advances* 6, eabd0511. https://doi.org/10.1126/sciadv.abd0511

Lodders, K. (2003) Solar System Abundances and Condensation Temperatures of the Elements. *The Astrophysical Journal* 591, 1220–1247. https://doi.org/10.1086/375492

Luais, B. (2012) Germanium chemistry and MC-ICPMS isotopic measurements of Fe–Ni, Zn alloys and silicate matrices: Insights into deep Earth processes. *Chemical Geology* 334, 295–311. https://doi.org/10.1016/j.chemgeo.2012.10.017

Luais, B., Florin, G. (2025) Origin of the mass-dependent germanium isotopic continuum in the early Solar System. *Earth and Planetary Science Letters* 672, 119663. https://doi.org/10.1016/j.epsl.2025.119663

Luck, J.-M., Othman, D.B., Albarède, F. (2005) Zn and Cu isotopic variations in chondrites and iron meteorites: Early solar nebula reservoirs and parent-body processes. *Geochimica et Cosmochimica Acta* 69, 5351–5363. https://doi.org/10.1016/j.gca.2005.06.018

Ni, P. (倪鹏), Macris, C.A., Darling, E.A., Shahar, A. (2021) Evaporation-induced copper isotope fractionation: Insights from laser levitation experiments. *Geochimica et Cosmochimica Acta* 298, 131–148. https://doi.org/10.1016/j.gca.2021.02.007

Nie, N.X., Chen, X.-Y., Hopp, T., Hu, J.Y., Zhang, Z.J., Teng, F.-Z., Shahar, A., Dauphas, N. (2021) Imprint of chondrule formation on the K and Rb isotopic compositions of carbonaceous meteorites. *Science Advances* 7, eabl3929. https://doi.org/10.1126/sciadv.abl3929

Nie, N.X., Chen, X.-Y., Zhang, Z.J., Hu, J.Y., Liu, W., Tissot, F.L.H., Teng, F.-Z., Shahar, A., Dauphas, N. (2023) Rubidium and potassium isotopic variations in chondrites and Mars: Accretion signatures and planetary overprints. *Geochimica et Cosmochimica Acta* 344, 207–229. https://doi.org/10.1016/j.gca.2023.01.004

Paquet, M., Moynier, F., Yokoyama, T., Dai, W., Hu, Y., *et al.* (2023) Contribution of Ryugu-like material to Earth's volatile inventory by Cu and Zn isotopic analysis. *Nature Astronomy* 7, 182–189. https://doi.org/10.1038/s41550-022-01846-1

Pringle, E.A., Moynier, F. (2017) Rubidium isotopic composition of the Earth, meteorites, and the Moon: Evidence for the origin of volatile loss during

planetary accretion. *Earth and Planetary Science Letters* 473, 62–70. https://doi.org/10.1016/j.epsl.2017.05.033

Rouxel, O.J., Luais, B. (2017) Germanium Isotope Geochemistry. *Reviews in Mineralogy and Geochemistry* 82, 601–656. https://doi.org/10.2138/rmg.2017.82.14

Wang, K., Jacobsen, S.B. (2016) Potassium isotopic evidence for a high-energy giant impact origin of the Moon. *Nature* 538, 487–490. https://doi.org/10.1038/nature19341

Wölfer, E., Burkhardt, C., Nimmo, F., Kleine, T. (2025a) Origin of moderately volatile elements in Earth inferred from mass-dependent Ge isotope variations among chondrites. *Earth and Planetary Science Letters* 663, 119435. https://doi.org/10.1016/j.epsl.2025.119435

Wölfer, E., Hellmann, J.L., Burkhardt, C., Kleine, T. (2025b) Ge, Te, and Zn isotopic link between Ryugu and CI chondrites. *Geochemical Perspectives Letters* 37, 1–6. https://doi.org/10.7185/geochemlet.2537

Zeng, H., Rozsa, V.F., Nie, N.X., Zhang, Z., Pham, T.A., Galli, G., Dauphas, N. (2019) Ab Initio Calculation of Equilibrium Isotopic Fractionations of Potassium and Rubidium in Minerals and Water. *ACS Earth and Space Chemistry* 3, 2601–2612. https://doi.org/10.1021/acsearthspacechem.9b00180

Zhang, Z., Grewal, D.S. (2026) A re-assessment of moderately volatile elements in the non-matrix component of carbonaceous chondrites. *Icarus* 452, 117049. https://doi.org/10.1016/j.icarus.2026.117049

Zhang, Z.J., Nie, N.X., Lin, C.Z. (2025) Potassium and rubidium isotopic analysis using Neoma MC-ICPMS with the collision/reaction cell. *Journal of Analytical Atomic Spectrometry* 40, 2945–2956. https://doi.org/10.1039/D5JA00189G

Zhu, K. (朱柯), Dai, B., Cao, X., Tian, S., Chen, L. (2025) O–Fe–Ti isotopic evidence for classifying Oued Chebeika 002 as a CI chondrite and its genetic affinities with CY chondrites, Ryugu, and Bennu. *Monthly Notices of the Royal Astronomical Society: Letters* 542, L7–L11. https://doi.org/10.1093/mnrasl/slaf059

Geochemical Perspectives Letters

K, Rb, Ge, and Cu isotopes in Oued Chebeika 002 compared with CI chondrites, Ryugu, and Bennu

D.S. Grewal, N.X. Nie, B. Luais, Z.J. Zhang, Q. Ahmad, A. Vazquez Ochoa, P. Ni

Supplementary Information

The Supplementary Information includes:

- Analytical Methods
- Tables S-1 and S-2
- Supplementary Information References

Analytical Methods

Major and trace elements. ~200 mg of bulk sample of Oued Chebeika 002 was crushed in an agate mortar that had been previously cleaned with diluted HNO_3, rinsed with 18.2 MΩ high-purity water, and dried with acetone under a laminar-flow hood (CRPG- Nancy). Part of the sample powder was analysed for major and trace elemental compositions at the SARM analytical facilities (Service Analytique des Roches et des Minéraux, CRPG-Nancy, France) following routine $LiBO_2$ alkaline fusion dissolution techniques and using a Thermo Fisher ICP-OES iCap Pro for major elements, and a Thermo Fisher ICP-MS iCapQ for trace elements (Table S-1). The Ge concentration in OC002 was determined using the standard addition method, to achieve better accuracy and high-precision measurements. Analytical details and errors on the measurements are given in Carignan *et al.* (2001).

K and Rb isotope measurements. The K and Rb chemical purification and isotopic analyses were carried out at the Cosmochemical Analysis and Testing (CAT) Laboratory at MIT. 45.9 mg of OC002 was ground using a cleaned agate mortar. The powder was digested in double-distilled HNO_3 + HF (2:1 v/v) at 130 °C on a hot plate for 48 hours, followed by repeated treatment with aqua regia (3:1 v/v HCl-HNO_3) until no visible precipitate remained. The sample was then dried, converted, and redissolved in 4 ml 1M HNO_3, ready for chromatographic separation.

The separation of K and Rb followed the "Sr resin method" described in Table 1 of Nie *et al.* (2021), with a minor modification. Specifically, a Ti-removal step was incorporated as the first step using the same column as Column 1 (16 ml AG50W-X8), and Column 2 of the original protocol was removed. This modification simplified the procedure by reusing the 16 ml AG50W-X8 resin without changing resins or columns for Ti removal. In the modified protocol, after cleaning, conditioning, and loading the samples, Column 1 was first eluted with 80 ml of 0.8M HNO_3 + 0.2M HF to remove matrix elements (Na, Fe, Ti, and Al), followed by collection of K and Rb in the subsequent 136 ml of the same acid mixture. The combined K/Rb fraction was dried and redissolved in 4 ml of 0.5M HNO_3, then reloaded onto the same column and eluted with 0.5M HNO_3 (corresponding to Column 1 in Nie *et al.*, 2021), followed by purification through Sr resin columns (Column 3 in Nie *et al.*, 2021). The Rb cut collected from Column 3 was processed repeatedly

when necessary, depending on the matrix-to-Rb ratio (particularly K/Rb), to ensure complete removal of residual matrix elements and obtain a pure Rb solution.

After purification, K and Rb isotopic compositions were measured using a Thermo Fisher Scientific Neoma multi-collector inductively coupled plasma mass spectrometer equipped with a pre-cell mass filter (MC-ICP-MS/MS) and a collision–reaction cell (CRC). Detailed analytical conditions, including cup configurations and tuning parameters, are reported in Zhang *et al.*, 2025). Potassium isotopes were analysed under dry plasma conditions using an APEX Ω desolvating nebulizer at a sample uptake rate of ~150 µL/min, with a standard Ni sampler cone and H-type skimmer cone. Measurements were performed in low-resolution mode with the MS/MS module operated at 10% magnetic field strength. A mixture of He and H_2 was introduced into the CRC to suppress ArH^+ interferences. Under these conditions, we obtained ~22 V for ^{39}K at concentrations of 50 ng/g, corresponding to a sensitivity of 440 V/ppm for ^{39}K.

Rubidium isotope measurements were conducted on the same instrument under dry plasma conditions using an APEX Ω desolvating nebulizer equipped with a standard Ni sampler cone and an X-type skimmer cone. Analyses were performed in low-resolution mode with the MS/MS module operated at 20 % magnetic field strength. Solutions were analysed at concentrations of 3-30 ng/g depending on Rb content in digested aliquots. We obtained ~4 V for ^{85}Rb at concentrations of 3 ng/g, corresponding to a sensitivity of 1333 V/ppm for ^{85}Rb.

Isotopic compositions are reported in per mil (‰) notation relative to SRM 999c for K and SRM 984 for Rb:

$$\delta^{41/39}K\ (‰) = [(^{41}K/^{39}K)_{sample} / (^{41}K/^{39}K)_{SRM\ 999c} - 1] \times 1000$$
$$\delta\ ^{87/85}Rb\ (‰) = [(^{87}Rb/^{85}Rb)_{sample} / (^{87}Rb/^{85}Rb)_{SRM\ 984} - 1] \times 1000$$

Uncertainties for individual samples are reported as 95 % confidence intervals and are based on repeated measurements (n = 3-12) of each sample solution, assuming a Student's t-distribution. Two geostandards (BCR-2 and AGV-2) were processed alongside the meteorite samples through the same chromatographic columns and analysed under identical conditions. For BCR-2, the measured isotope compositions are $\delta^{41/39}K = -0.446 \pm 0.040$ ‰ (n = 8) and $\delta^{87/85}Rb = -0.210 \pm 0.030$ ‰ (n = 10), which agree within uncertainty with literature values ($\delta^{41/39}K = -0.49$ ‰; Wang *et al.*, 2021; $\delta^{87/85}Rb = -0.16$ ‰; Nie *et al.*, 2021). For AGV-2, the measured values are $\delta^{41/39}K = -0.452 \pm 0.083$ ‰ (n = 6) and $\delta^{87/85}Rb = -0.160 \pm 0.034$ ‰ (n = 12), also consistent with published values ($\delta^{41/39}K = -0.45$ ‰; Wang *et al.*, 2021; $\delta^{87/85}Rb = -0.15$ ‰; Nie *et al.*, 2021).

Ge isotopic measurements. The Ge chemistry and isotopic measurements were performed on an aliquot of the same OC002 sample powder used for the major and trace element analyses. The protocol for sample digestion and matrix separation is specific to Ge chemistry and follows the methods described in Ahmad *et al.* (2026); Luais (2007, 2012); and Luais and Florin (2025). All chemical reagents used were high-purity HF and HNO_3 acids from SeaStar™ and 18.2 MΩ deionised water. All steps of chemistry were carried out in the ISO-6 IRISS clean-lab facilities at CRPG-Nancy (France).

We analysed the OC002 sample along with the previously characterised CV-type Allende chondrite and the BIR-1 geostandard (Icelandic basalt) to assess analytical accuracy and reproducibility. Because of the high carbon contents (at the percent level) in CI-type and carbonaceous chondrites, we performed a pre-digestion heating of the chondrite samples at 600 °C in a furnace in platinum crucibles for carbon combustion (Luais and Florin, 2025). The chondrite and BIR-1 sample powders were then digested in 3:1 mixtures of concentrated HF and HNO_3 acids in screw-top Teflon vials on a hot plate at 65 °C to avoid any loss of volatile Ge. Alternating ultrasonic and hot plate steps were applied over several days until a whitish, cloudy solution free of any visible particles was obtained, resulting from the formation of Al-Mg-Ca-fluorides that do not incorporate Ge (Luais, 2012). A final centrifugation step ensured complete recovery of Ge in the supernatant solution.

After evaporation to dryness, the residue was dissolved in 1M HF for subsequent germanium isolation using a combined double-stack resin-exchange chromatography column (Luais, 2012; Ahmad *et al.*, 2026). This technique enables collection of a pure Ge fraction in a single chromatographic sequence. The procedure consists of loading the 1M HF sample solution onto an AG 1-X8 anion exchange resin, followed by additional 1M HF to elute the matrix. After placing an AG 50W-X8 cation-exchange resin column beneath the anionic column, 5 ml of 0.2M HNO_3 is passed through both columns to elute germanium. After removing the AG 1-X8 anion exchange column, an additional 2 ml of

0.5M HNO_3 is passed through the AG 50W-X8 cation-exchange resin to ensure complete Ge purification and recovery.

Ge isotopic measurements were conducted at CRPG using a Neptune Plus MC-ICP-MS coupled with a Cetac HGX-200 hydride generator introduction system (HGIS) with an uptake rate of ~200 µl·min^{-1} (Rouxel and Luais, 2017; Florin *et al.*, 2020). This technique eliminates isobaric interferences from elements that do not form hydrides (*e.g.*, Zn, Fe, Ni), thereby avoiding matrix effects. It provides a gain in signal sensitivity of at least a factor of 30, enabling measurement of very low quantities of Ge at the tens-of-ppb level with the high precision required for routine isotopic measurements of 10-20 ng Ge. At the beginning of each analytical session, gas flow rates, torch parameters, and ion lenses were optimised using a solution of the NIST SRM 3120a Ge standard (Luais, 2012). Gain calibration between the Faraday cups was performed prior to optimising peak shapes and centering the peaks. Analyses were carried out on diluted 10 ppb samples and standard solutions, with beam intensities matching to within 7% between samples and standards, giving an average ^{74}Ge beam intensity of 2 V during the course of this study. Typical acquisition sequences consisted of alternating measurements of the NIST SRM 3120a Ge standard and samples, with a washout time of 200 s in 0.5M HNO_3 between standard and samples. Data acquisition consisted of 40 integration cycles measured during 8.4 s, yielding an internal precision better than 5 ppm/amu (2SE).

This configuration allows calculation of Ge isotope ratios using the standard-bracketing method, expressed in delta notation relative to the NIST SRM 3120a Ge standard measured before and after each sample:

$$\delta^{74/70}\text{Ge (‰)} = [(^{74}\text{Ge}/^{70}\text{Ge})_{\text{sample}} / (^{74}\text{Ge}/^{70}\text{Ge})_{\text{NIST 3120a}} - 1] \times 1000$$

The total Ge procedural blanks, including chemistry and MC-ICP-MS measurements, were <0.2 ng, representing 0.04% of chemically processed Ge; therefore, no blank correction was applied.

The JMC and Aldrich Ge standards, as well as the BIR-1 geostandard (Luais, 2012) were used as secondary standards to evaluate the long-term stability, accuracy, and precision of isotopic measurements (Table S-2). Average values for the JMC and Aldrich Ge standard solutions yielded $\delta^{74/70}$Ge = −0.299 ± 0.093 ‰ (n = 13) and $\delta^{74/70}$Ge = −1.968 ± 0.119 ‰ (n = 16), respectively (2σ SD). The BIR-1 basalt yielded $\delta^{74/70}$Ge = 0.65 ± 0.12‰ (n = 5), while the CV-type Allende meteorite and its reference material gave $\delta^{74/70}$Ge = 0.093 ± 0.073 ‰ (n =6), and 0.08 ± 0.100 ‰ (n=6), respectively (Table S-1). All results are consistent within 2 standard deviations with published reference values (Luais, 2012; Luais and Florin, 2025; Ahmad *et al.*, 2026). At least five replicates were required to achieve external reproducibility of ~0.1 ‰ (2σ SD).

Cu isotopic measurements. ~4 mg of the OC002 aliquot was dissolved overnight on a hot plate in a 2:1 mixture of concentrated HF and HNO_3 for Cu isotope analysis. The dissolved solution was dried down and converted to chloride form, then dissolved in 8M HCl for Cu column purification. Copper separation was conducted using BioRad quartz glass columns with a diameter of 0.5 cm. Each column was filled with approximately 5 cm of BioRad AG1-X8 (200-400 mesh) resin. Matrix elements were eluted using 6.5 ml of 8M HCl, and the Cu fraction was subsequently eluted in another 9.5 ml of 8M HCl. The purification process was repeated once to further purify Cu. The final products were converted to nitric form and dissolved in 2% nitric acid for mass spectrometer analysis.

Copper isotope analysis was performed under high-energy mode on a Nu Sapphire collision-cell multi-collector inductively coupled plasma mass spectrometer (MC-ICP-MS) at UCLA. Sample aliquots were diluted to 50 ppb and introduced into the mass spectrometer in wet plasma mode. The sensitivity was approximately 30 V/ppm at a sample introduction rate of 60 µL/min. Standard-sample bracketing using the ERM-AE633 standard was used to correct for instrumental mass bias. Each sample was measured 6 times, with each measurement consisting of 30 cycles with 4 seconds of integration. Variations in Cu ratios are reported relative to the international standard SRM976 after correcting for a −0.01‰ difference between SRM976 and ERM-AE633 (Moeller *et al.*, 2012).

$$\delta^{65/63}\text{Cu (‰)} = [(^{65}\text{Cu}/^{63}\text{Cu})_{\text{sample}} / (^{65}\text{Cu}/^{63}\text{Cu})_{\text{SRM 976}} - 1] \times 1000$$

A geological standard, AGV-2, was analysed along with OC002 to verify the external precision of the session. A $\delta^{65/63}$Cu value of 0.036 ± 0.024‰ (2SE, n = 6) was obtained for AGV-2, consistent with the recommended value of 0.04 ± 0.04 ‰ (Moynier *et al.*, 2017).

Supplementary Tables

Table S-1 Bulk element abundances in Oued Chebeika 002 (in wt. % for major elements and Ni, and in µg/g for the other elements).

Oued Chebeika 002			
SiO_2	25.11	**Pb**	2.46
Al_2O_3	1.56	**Rb**	2.34
Fe_2O_3 Total	28.20	**Sb**	0.438
MnO	0.319	**Sc**	6.12
MgO	17.50	**Sn**	1.55
CaO	1.89	**Sr**	9.72
Na_2O	0.75	**Ta**	0.017
K_2O	0.063	**Th**	0.029
TiO_2	0.079	**U**	0.010
P_2O_5	0.15	**V**	49.8
LOI	n.d.	**W**	0.328
		Y	1.15
As	1.63	**Zn**	341
Ba	< L.D.	**Zr**	5.5
Be	< L.D.	**La**	0.232
Bi	0.118	**Ce**	0.606
Cd	0.71	**Pr**	0.084
Co	516	**Nd**	0.423
Cr	2737	**Sm**	0.135
Cs	0.172	**Eu**	0.050
Cu	*216* *	**Gd**	0.170
Ga	11.2	**Tb**	0.032
Ge	36.5	**Dy**	0.209
Hf	0.142	**Ho**	0.049
In	0.099	**Er**	0.129
Mo	1.24	**Tm**	0.021
Nb	0.269	**Yb**	0.131
Ni %	1.04	**Lu**	0.020

n.d. : not determined

< L.D. : under the detection limit

* The measured Cu concentration (216 ppm) is well above the 107 ppm obtained by isotope dilution and exceeds the range of other CI chondrites, Ryugu, and Bennu (~108-156 ppm). We currently have no explanation for this discrepancy. We use the isotope-dilution value of 107 ppm in all figures.

Table S-2 Germanium isotopic compositions of Oued Chebeika 002, and Allende (CV), BIR-1 samples, secondary Ge standard solutions analysed during the course of this study.

	Reference	n	$\delta^{72/70}$Ge	±2σ SD	$\delta^{73/70}$Ge	±2σ SD	$\delta^{74/70}$Ge	±2σ SD	***	$\delta^{74/70}$Ge	±2σ SD
Oued Chebeika 002 (CI)		5	0.513	0.015	0.727	0.072	0.980	0.067	Orgueil (CI)	0.901 [1]	0.057
Allende (CV) *	MNHN02811	6	0.058	0.034	0.069	0.070	0.093	0.073	Allende	0.096 [1]	0.120
Allende (CV) RM**	USNM 3529	6	0.045	0.057	0.056	0.089	0.080	0.100			
BIR-1 geostandard		5	0.362	0.104	0.504	0.112	0.65	0.125	BIR-1	0.612 [1] 0.61 [2]	0.095 0.09
Secondary std solutions											
JMC Ge Standard		13	-0.140	0.044	-0.183	0.039	-0.299	0.093	n= 67	-0.309	0.095
Aldrich Ge Standard		16	-1.014	0.059	-1.515	0.095	-1.968	0.119	n =68	-1.967	0.090

* Muséum National d'Histoire Naturelle Paris

** Smithsonian Institution of Washington, Reference material, split15, position 24

*** [1] Luais and Florin (2025); [2] Ahmad *et al*. (2026)

Supplementary Information References

Ahmad, Q., Cividini, D., Luais, B. (2026) A fast double-stack chromatographic separation of germanium from silicate material for isotope analysis with MC-ICP-MS. *Journal of Analytical Atomic Spectrometry* 41, 935–941. https://doi.org/10.1039/D5JA00471C

Carignan, J., Hild, P., Mevelle, G., Morel, J., Yeghicheyan, D. (2001) Routine Analyses of Trace Elements in Geological Samples using Flow Injection and Low Pressure On-Line Liquid Chromatography Coupled to ICP-MS: A Study of Geochemical Reference Materials BR, DR-N, UB-N, AN-G and GH. *Geostandards Newsletter* 25, 187–198. https://doi.org/10.1111/j.1751-908X.2001.tb00595.x

Florin, G., Luais, B., Rushmer, T., Alard, O. (2020) Influence of redox processes on the germanium isotopic composition of ordinary chondrites. *Geochimica et Cosmochimica Acta* 269, 270–291. https://doi.org/10.1016/j.gca.2019.10.038

Luais, B. (2007) Isotopic fractionation of germanium in iron meteorites: Significance for nebular condensation, core formation and impact processes. *Earth and Planetary Science Letters* 262, 21–36. https://doi.org/10.1016/j.epsl.2007.06.031

Luais, B. (2012) Germanium chemistry and MC-ICPMS isotopic measurements of Fe–Ni, Zn alloys and silicate matrices: Insights into deep Earth processes. *Chemical Geology* 334, 295–311. https://doi.org/10.1016/j.chemgeo.2012.10.017

Luais, B., Florin, G. (2025) Origin of the mass-dependent germanium isotopic continuum in the early Solar System. *Earth and Planetary Science Letters* 672, 119663. https://doi.org/10.1016/j.epsl.2025.119663

Moeller, K., Schoenberg, R., Pedersen, R.-B., Weiss, D., Dong, S. (2012) Calibration of the New Certified Reference Materials ERM-AE633 and ERM-AE647 for Copper and IRMM-3702 for Zinc Isotope Amount Ratio Determinations. *Geostandards and Geoanalytical Research* 36, 177–199. https://doi.org/10.1111/j.1751-908X.2011.00153.x

Moynier, F., Vance, D., Fujii, T., Savage, P. (2017) The Isotope Geochemistry of Zinc and Copper. *Reviews in Mineralogy and Geochemistry* 82, 543–600. https://doi.org/10.2138/rmg.2017.82.13

Nie, N.X., Chen, X.-Y., Hopp, T., Hu, J.Y., Zhang, Z.J., Teng, F.-Z., Shahar, A., Dauphas, N. (2021) Imprint of chondrule formation on the K and Rb isotopic compositions of carbonaceous meteorites. *Science Advances* 7, eabl3929. https://doi.org/10.1126/sciadv.abl3929

Rouxel, O.J., Luais, B. (2017) Germanium Isotope Geochemistry. *Reviews in Mineralogy and Geochemistry* 82, 601–656. https://doi.org/10.2138/rmg.2017.82.14

Wang, K. (王昆), Li, W., Li, S., Tian, Z., Koefoed, P., Zheng, X.-Y. (2021) Geochemistry and cosmochemistry of potassium stable isotopes. *Geochemistry* 81, 125786. https://doi.org/10.1016/j.chemer.2021.125786

Zhang, Z.J., Nie, N.X., Lin, C.Z. (2025) Potassium and rubidium isotopic analysis using Neoma MC-ICPMS with the collision/reaction cell. *Journal of Analytical Atomic Spectrometry* 40, 2945–2956. https://doi.org/10.1039/D5JA00189G